

Murray's Law as an Entropy-per-Information-Cost Extremum

Justin Bennett^{1,*}

¹*Department of Physics, University of Illinois Urbana-Champaign, Urbana, Illinois 61801, USA[†]*

(Dated: November 14, 2025)

Any vascular or transport network must continuously pay two energetic bills: the power dissipated to drive flow and the ongoing cost of building and maintaining reliably decodable structure. This tradeoff is formulated here as an entropy-per-information-cost (EPIC) variational principle that prices structural upkeep in absolute energetic units (J/bit), from which Murray's law and its angular counterpart emerge as stationarity conditions. In the Poiseuille regime, equal-marginal-price stationarity yields the branchwise invariant

$$\frac{Q_i^2}{c_i r_i^{m+4}} = \text{const},$$

so that $Q \propto r^\alpha$ with $\alpha = (m + 4)/2$ and the tariff-weighted Murray relation

$$\sqrt{c_0} r_0^\alpha = \sqrt{c_1} r_1^\alpha + \sqrt{c_2} r_2^\alpha.$$

Homogeneous tariffs recover the classical cubic law when upkeep is volume-priced ($m = 2 \Rightarrow \alpha = 3$), while surface-priced upkeep gives $\alpha = 5/2$. Translational stationarity fixes branch directions via the tariff-weighted vector closure

$$\sum_{i=0}^2 c_i r_i^m \mathbf{e}_i = 0,$$

predicting near-symmetric daughter openings of 74.93° for $m = 2$ and 97.44° for $m = 1$; notably, this angle law is independent of hydraulic exponent n . Pricing dissipation at an audited effective bit energy ε_b furnishes a unit-bearing, domain-level growth bound on the instantaneous rate of creating reliably decodable structure,

$$\dot{I} \leq \min \left\{ \int_V \sigma_s T / \varepsilon_b dV, \int_\Sigma C_\epsilon dA \right\}.$$

Under homogeneous tariffs, the same extremum enforces a universal power split $nP_{\text{flow}} = mP_{\text{struct}}$ and, after eliminating radii, an effective per-length edge cost $\propto [\varepsilon_b c]^{n/(m+n)} Q^{2m/(m+n)}$, which is strictly concave for $m < n$ and thereby favors tree-like mergers. Spatial heterogeneity defines an EPIC index $\mathfrak{n}(x) \propto [\varepsilon_b(x)c(x)]^{n/(m+n)}$ that induces Snell-type refraction, $\mathfrak{n}_1 \sin \theta_1 = \mathfrak{n}_2 \sin \theta_2$, across tariff jumps. On High-Resolution Fundus (HRF) images ($N = 19,127$ junctions), the held-out vector-closure residual has median 0.213 (bootstrap 95% CI [0.209, 0.217]) and is strongly left-shifted relative to four structure-preserving nulls, stable under 10% radius jitter and QC ablations. Together, these unit-consistent statements supply concrete, falsifiable targets: audit ε_b and structural tariffs c_i , perturb surface/volume pricing to shift α and symmetric angles as predicted, and engineer spatial price contrasts to test refraction in controlled geometries.

I. INTRODUCTION

Nature channels free energy through architectural pathways that must be continually maintained, and the energetic burden of that upkeep is repaid by an increased *entropy-production rate*—the rate at which irreversible processes create entropy in the medium, integrated over the relevant volume [1–4]. At laminar bifurcations this exchange leaves a distinctive geometric fingerprint: Murray's law, the empirically robust and repeatedly rederived statement that the parent and two daughter radii satisfy a cubic relation [5–8]. The tension is classical: narrowing a channel drives viscous losses steeply upward, while enlarging it imposes a standing metabolic toll for fabricating, perfusing, and maintaining tissue. Between these opposing costs lies an

operating point—wide enough to tame dissipation, not so wide that upkeep dominates.

This paper advances a simple claim: the canonical cubic form of Murray's law, together with its surface-weighted generalizations, emerges as the stationarity condition of a single, empirically calibratable *entropy-per-information-cost* (EPIC) variational principle, whose geometric and dynamical predictions are tested against biological data. The analysis proceeds in the Poiseuille regime, where steady, isothermal Newtonian flow isolates the trade-off between viscous dissipation and the energetic cost of maintaining structure at a single branching site. In this near-equilibrium setting—one parent conduit feeding two daughters with fixed demands, $Q_0 = Q_1 + Q_2$ —the Y-junction functions as a controlled laboratory: infinitesimal changes in radii and branch angles map linearly, via the Hagen-Poiseuille law, to power expenditure, enabling sharp, falsifiable tests of EPIC's predictions against empirical morphologies and fluxes.

Against this backdrop, the aim here is not to promulgate a new law of transport but to supply a principled accounting for the law that already governs these systems. In the EPIC formulation,

* jmb15@illinois.edu

[†] Independent work; not conducted under, nor funded by, the University of Illinois research program.

the familiar calculus of nonequilibrium thermodynamics is recast in an informational currency: the reliably maintained distinctions that keep a conduit operative are priced in absolute energetic units through an *effective bit tariff* $\varepsilon_b = \zeta k_B T \ln 2$, anchored in Landauer’s bound that each reliably executed bit dissipates at least $k_B T \ln 2$ of work [9]. Expressed in these units, the local dissipation $\sigma_s T$ functions as a spendable budget of reliably decodable information, $\Psi_b \equiv \sigma_s T / \varepsilon_b$ [bit/(m³ s)]. The underlying hydrodynamics remain unchanged; what shifts is the objective: geometry is determined by a constrained ledger that extremizes entropy production *per unit information cost*, rather than by appealing to any global “maximum entropy production” maxim. In the special case of a uniform tariff and a geometry-independent structural bit budget, this variational principle reduces to the classical minimum-power design at fixed daughter flows, recovering the canonical cubic form of Murray’s law. Definitions, units, and notation are summarized in the *Notation and units (quick reference)* (§VIII).

From this vantage, three principled consequences organize what follows. First, the equal-marginal-price stationarity condition fixes, on each branch i , a “priced–flux” invariant,

$$\frac{Q_i^2}{c_i r_i^{m+4}} = \text{const},$$

so that $Q \propto r^\alpha$ with $\alpha = (m+4)/2$; enforcing continuity at the node then yields the tariff-weighted Murray relation

$$\sqrt{c_0} r_0^\alpha = \sqrt{c_1} r_1^\alpha + \sqrt{c_2} r_2^\alpha,$$

which reduces to the classical cubic law $r_0^3 = r_1^3 + r_2^3$ under homogeneous (volume-priced) tariffs ($m = 2$) and to its surface-priced analogue with $\alpha = 5/2$ when boundary costs dominate. Second, translational neutrality of the optimum implies the tariff-weighted vector closure $\sum_i c_i r_i^m \mathbf{e}_i = 0$, fixing the daughter opening angle; in the near-symmetric limit this recovers the familiar $\sim 75^\circ$ arterial bifurcation and furnishes a crisp, image-level test. Third, expressing dissipation in units of reliably decodable information yields a two-faced “growth-cone” bound on the rate of creating robust structure (see Methods for a short proof and assumptions A1–A4),

$$I \leq \min \left\{ \int_V \Psi_b dV, \int_\Sigma C_\varepsilon dA \right\},$$

so that the limiting mechanism is legible: either the interior power budget (via $P_{\text{flow}}/\varepsilon_b$) or the boundary’s reliable throughput.

The same homogeneity that underlies these results yields compact design rules. Under uniform dilation of all radii, the objective enforces a universal power split $n P_{\text{flow}} = m P_{\text{struct}}$. Eliminating radii produces an effective per-length cost $\propto [\varepsilon_b c]^{n/(m+n)} Q^{2m/(m+n)}$, whose strict concavity ($2m/(m+n) < 1$) explains the ubiquity of tree-like mergers. Finally, spatial gradients of the EPIC index $n \propto [\varepsilon_b c]^{n/(m+n)}$ enforce a Snell-type relation $n_1 \sin \theta_1 = n_2 \sin \theta_2$, predicting systematic bending toward cheaper-tariff regions. These analytically sharp, testable statements frame the empirical sections that follow.

II. THE EPIC LEDGER: ENERGETIC TARIFFS, STRUCTURAL LOAD, AND INFORMATION THROUGHPUT

The EPIC ledger places energy use and morphology on a single, measurable footing by expressing both in a common unit: the reliably decoded bit—here understood in the operational sense of a single, reproducible binary decision (e.g., open/closed, high/low) resolved over a specified time window at a declared error tolerance. Three primitives effect this change of variables. An *information tariff* assigns an absolute energetic price to each such bit; a *structural bit-rate* counts the rate at which a network must refresh, monitor, and stabilize its conduits; and a *power-priced information throughput* re-expresses local dissipation as the rate at which reliable distinctions can, in principle, be maintained. Expressed in a common unit, energetic supply and informational demand are placed on the same quantitative footing, fixing the scale for all subsequent variational statements and enabling direct, testable links between geometry, power, and information.

The tariff is quantified by the effective bit energy

$$\varepsilon_b = \zeta k_B T \ln 2, \quad \eta_b \equiv \varepsilon_b^{-1},$$

with T the (locally) isothermal audit temperature and $\zeta \geq 1$ aggregating finite-time, reliability, redundancy, and housekeeping overheads (cf. Landauer’s bound $k_B T \ln 2$ per reliable bit [9]). Operationally, ε_b is the measured ratio of baseline-subtracted control-layer power to the stream of reliably decoded bits at the chosen error tolerance; its reciprocal η_b converts power density into an information-throughput density $\Psi_b \equiv \sigma_s T / \varepsilon_b$ [bit m⁻³ s⁻¹], so that the familiar dissipation $\sigma_s T$ is read as the rate of reliable information available to sustain structure.

On the demand side, the rate at which a branching conduit must maintain distinctions along a segment of radius r_i and length l_i is modeled as

$$\mathcal{B}(\mathbf{r}) = \sum_{i=0}^2 c_i l_i r_i^m, \quad [\mathcal{B}] = \text{bit s}^{-1},$$

where the positive coefficients c_i encode platform-specific sensing, control, and refresh burdens per unit surface or volume, and the exponent m captures how upkeep scales with size: $m = 2$ for volume-priced maintenance and $m = 1$ for surface-priced burdens.

Pricing dissipation at the audited tariff defines the *power-priced* throughput,

$$\Psi_b = \frac{\sigma_s T}{\varepsilon_b} \quad (\text{bit m}^{-3} \text{ s}^{-1}),$$

which recasts each watt of irreversible power as η_b bits per second of maintainable information. In a steady, isothermal control volume V ,

$$\int_V \Psi_b dV = \frac{\int_V \sigma_s T dV}{\varepsilon_b} = \frac{P_{\text{flow}}}{\varepsilon_b},$$

so the hydraulic power P_{flow} is read directly in bit s⁻¹ at the audited price ε_b . Because σ_s and T arise from transport while

ε_b is measured by an explicit control-layer audit, Ψ_b is both physically grounded and experimentally accessible.

In this form, the EPIC ledger makes the design problem explicit: geometry is selected by balancing an audited supply of reliable information $\int \Psi_b$ against the structural demand \mathcal{B} , i.e., by extremizing entropy throughput per unit information cost under the required maintenance load. The auditing protocol (choice of time window τ), the decomposition of ζ , and reporting conventions are detailed in §VIII.

III. CLASSICAL BENCHMARK: PUMPING POWER VERSUS UPKEEP AT FIXED DEMAND

Before introducing the EPIC ledger, it is helpful to recall the classical optimization that balances viscous pumping power against an explicit upkeep cost at *fixed* daughter demands. Consider a single Y-junction in which one parent segment (r_0, ℓ_0) feeds two daughters (r_1, ℓ_1) and (r_2, ℓ_2) . The fluid is taken incompressible and Newtonian; flow is steady, laminar, and fully developed in long circular tubes (entrance effects neglected). Under these conditions each segment obeys the Hagen–Poiseuille relations

$$Q_i = \frac{\pi r_i^4}{8\mu\ell_i} \Delta p_i, \quad P_{\text{flow},i} = Q_i \Delta p_i = \frac{8\mu\ell_i}{\pi} \frac{Q_i^2}{r_i^4}, \quad (1)$$

with dynamic viscosity μ and volumetric flow Q_i (see, e.g., White and Bruus [10, 11]). Throughout this benchmark, daughter demands are prescribed so that $Q_0 = Q_1 + Q_2$ and segments are isothermal. As a contrasting ensemble, note that if Δp were fixed at the node, no nontrivial optimum in the radii would exist, since $P_{\text{flow}} \propto r^4$ would grow monotonically with size [1].

To represent the standing energetic burden of keeping a patent conduit and its working fluid available, introduce an upkeep power that scales as a power of radius,

$$P_{\text{maint},i} = \Lambda_m \ell_i r_i^m, \quad m = \begin{cases} 2, & \text{volume-priced,} \\ 1, & \text{surface-priced,} \end{cases}$$

with $\Lambda_m > 0$. At fixed Q_i the per-segment objective separates,

$$P_i(r_i) = \frac{8\mu\ell_i}{\pi} \frac{Q_i^2}{r_i^4} + \Lambda_m \ell_i r_i^m, \quad (2)$$

so each radius can be optimized independently of the others given its prescribed flow. In the classical benchmark, Λ_m is an *ad hoc* scale that stands in for the price of keeping structure. The EPIC formulation makes this term *physical* by replacing $\Lambda_m \ell_i r_i^m$ with an *audited* cost $\varepsilon_b c_i \ell_i r_i^m$, where ε_b (J/bit) is measured from control-layer power and reliably decoded bit-rate, and $c_i r_i^m$ counts the *structural bit-rate* demanded by geometry, as overviewed in the next section.

Stationarity of (2) at fixed Q_i gives

$$\frac{dP_i}{dr_i} = -\frac{32\mu\ell_i}{\pi} \frac{Q_i^2}{r_i^5} + m \Lambda_m \ell_i r_i^{m-1} = 0,$$

hence the branchwise invariant

$$\frac{Q_i^2}{r_i^{m+4}} = \frac{\pi m \Lambda_m}{32\mu} \implies \boxed{Q_i \propto r_i^\alpha, \quad \alpha = \frac{m+4}{2}}. \quad (3)$$

Imposing continuity $Q_0 = Q_1 + Q_2$ then yields the generalized Murray family

$$\boxed{r_0^\alpha = r_1^\alpha + r_2^\alpha, \quad \alpha = \frac{m+4}{2}}. \quad (4)$$

Thus the classical cubic law $r_0^3 = r_1^3 + r_2^3$ arises when upkeep is volume-priced ($m = 2$), while $\alpha = 5/2$ characterizes a surface-priced burden ($m = 1$) [5–8, 12, 13].

The optimizer is unique. Indeed,

$$\frac{d^2 P_i}{dr_i^2} = \frac{160\mu\ell_i}{\pi} \frac{Q_i^2}{r_i^6} + m(m-1)\Lambda_m \ell_i r_i^{m-2} > 0$$

for $r_i > 0$ and $m \in \{1, 2\}$. Moreover, multiplying the first-order condition by r_i exposes a transparent power partition at the optimum,

$$4 P_{\text{flow},i} = m P_{\text{maint},i} \implies P_{\text{flow},i} = \frac{m}{4} P_{\text{maint},i},$$

i.e., $P_{\text{flow}} = \frac{1}{2} P_{\text{maint}}$ for $m = 2$ and $P_{\text{flow}} = \frac{1}{4} P_{\text{maint}}$ for $m = 1$. Note that ℓ_i cancels from the stationarity condition, so (3)–(4) hold even when the segment lengths differ.

The validity domain of this benchmark is that of (1): steady laminar flow of a Newtonian fluid in long circular tubes. Outside this regime, the same variational structure can be revisited with the appropriate dissipation law; for example, in small vessels the apparent viscosity depends on radius (Fåhræus–Lindqvist effect), $\mu \rightarrow \mu(r)$, which shifts the effective exponent while preserving the optimization logic [14–16].

Finally, this classical *pumping + upkeep* calculation fixes the essentials of the node problem used throughout: the ensemble (fixed Q_1, Q_2 , isothermal), a separable per-segment objective at fixed flow, a unique interior optimum with $Q \propto r^{(m+4)/2}$, and the additive law $r_0^\alpha = r_1^\alpha + r_2^\alpha$. Crucially, the only *modeling* element here is the upkeep scale Λ_m in $\Lambda_m \ell_i r_i^m$. EPIC seeks to replace this ad hoc scale by an *audited* pair (ε_b, c_i) and the priced objective

$$P_{\text{flow}} + \Lambda \mathcal{B}, \quad \mathcal{B} = \sum_i c_i \ell_i r_i^m, \quad \Lambda = \lambda \varepsilon_b,$$

so that upkeep is expressed in calibrated units (J/bit) and counted as a structural bit-rate. When ε_b is uniform and \mathcal{B} is held fixed across admissible variations, the EPIC extremum reduces to the same minimum-power design at fixed daughter flows.

IV. EPIC EXTREMUM: ENTROPY PER INFORMATION COST

With the classical benchmark in hand, the EPIC extremum changes only the *accounting*, not the physics. Transport dissipation and structural upkeep are expressed in a single, audited

currency: entropy production—priced at an effective bit energy—pays for the reliably maintained distinctions that keep channels operative. Specializing this domain-level ledger to a steady Y-junction at fixed daughter demands yields a node objective whose Euler–KKT conditions do the essential work: the equal–marginal–price stationarity recovers $Q \propto r^{(m+4)/2}$ and the tariff-weighted Murray relation; translating the junction enforces a tariff-weighted vector closure that fixes the branch angles; and, within the same calculus, per-segment power partitions, coordinate-free diagnostics, and rheological generalizations fall out naturally. The subsections that follow make this progression explicit: (i) domain program \rightarrow node objective, (ii) equal-marginal-price condition, (iii) branch invariant and weighted Murray law, and (iv) angle selection by translation, with extensions collected at the end of the section.

A. Domain program to node objective

At the level of a space–time domain \mathcal{D} , the design question is to choose a geometry that trades interior dissipation against the energetic price of maintaining reliable structure—expressed in a single, audited currency. This trade is written as an energy functional,

$$\delta \left[\int_{\mathcal{D}} \sigma_s T dV dt + \lambda \int_{\mathcal{D}} \varepsilon_b \beta dV dt \right] = 0, \quad \lambda \geq 0,$$

where σ_s is the local entropy–production density, T the node–isothermal audit temperature, and β the density of reliably executed bit–operations. Both integrals carry units of energy: the first is the energy dissipated by transport within \mathcal{D} , the second is the energy *spent* to sustain reliably decodable structure at the audited price ε_b (J/bit). The multiplier λ is therefore dimensionless: it regulates the exchange rate between “watts of dissipation” and “watts dedicated to reliable bits” in the extremum.

For a single, steady, isothermal node with uniform ε_b , the spacetime ledger factorizes over an audit window of duration τ : $\int_{\mathcal{D}} \sigma_s T dV dt = \tau P_{\text{flow}}$ and $\int_{\mathcal{D}} \varepsilon_b \beta dV dt = \tau \varepsilon_b \mathcal{B}$, where P_{flow} is the hydraulic (dissipated) power and $\mathcal{B} = \sum_{i=0}^2 c_i \ell_i r_i^m$ is the structural bit–rate demanded by the geometry; dividing by τ and absorbing the tariff into $\Lambda \equiv \lambda \varepsilon_b > 0$ yields the node-level objective

$$\mathcal{L}(\mathbf{r}) = P_{\text{flow}}(\mathbf{r}) + \Lambda \mathcal{B}(\mathbf{r}), \quad (5)$$

posed at fixed daughter demands Q_1, Q_2 with $Q_0 = Q_1 + Q_2$. In this steady setting both terms carry units of power, so the geometry \mathbf{r} is chosen to balance a priced supply of reliable information ($\Lambda \mathcal{B}$) against the hydraulic cost (P_{flow}); an equivalent isoperimetric (ratio) program that maximizes entropy throughput *per* information cost is mathematically identical and leads to the same Euler–KKT conditions. Stationarity of (5) with respect to each radius then enforces

$$\frac{\partial P_{\text{flow}}}{\partial r_i} + \Lambda \frac{\partial \mathcal{B}}{\partial r_i} = 0 \quad (i = 0, 1, 2), \quad (6)$$

which states that, at the optimizer, the marginal reduction in pumping power from an infinitesimal change in r_i is exactly offset by the tariff-priced marginal increase in structural load—the equal-marginal-price rule.

B. Branch invariant and weighted Murray (Poiseuille)

In the Poiseuille regime each branch carries a per-length hydraulic cost $P_{\text{flow},i} = (8\mu \ell_i / \pi) Q_i^2 r_i^{-4}$ and a priced structural load $\mathcal{B}_i = c_i \ell_i r_i^m$. Substituting these into the stationarity condition (6) and cancelling the common length $\ell_i > 0$ yields an equal–marginal–price balance that condenses to the branchwise invariant

$$\frac{Q_i^2}{c_i r_i^{m+4}} = \kappa, \quad \kappa \equiv \frac{\pi m \Lambda}{32 \mu} > 0, \quad (7)$$

which is independent of segment length and has units $[\kappa] = \text{m}^3 \text{s}^{-1} \text{bit}^{-1}$. Solving (7) gives the flow–radius scaling

$$Q_i = \kappa^{1/2} \sqrt{c_i} r_i^\alpha, \quad \alpha = \frac{m+4}{2}, \quad (8)$$

and enforcing continuity $Q_0 = Q_1 + Q_2$ at the node produces the tariff-weighted Murray relation

$$\sqrt{c_0} r_0^\alpha = \sqrt{c_1} r_1^\alpha + \sqrt{c_2} r_2^\alpha.$$

Under homogeneous tariffs $c_0 = c_1 = c_2$ this collapses to the familiar additive family $r_0^\alpha = r_1^\alpha + r_2^\alpha$; in particular, volume-priced upkeep ($m = 2$) gives $\alpha = 3$ (the classical cubic law) and surface-priced upkeep ($m = 1$) gives $\alpha = 5/2$.

The same Euler condition exposes a transparent power partition. Multiplying (6) by r_i and using the definitions above,

$$4 P_{\text{flow},i} = m \Lambda c_i \ell_i r_i^m \equiv m P_{\text{struct},i},$$

so each branch satisfies $P_{\text{flow},i} = (m/4) P_{\text{struct},i}$. Summing over branches gives the global split $P_{\text{flow}} = \frac{1}{2} P_{\text{struct}}$ for $m = 2$ and $P_{\text{flow}} = \frac{1}{4} P_{\text{struct}}$ for $m = 1$ (with $P_{\text{struct}} \equiv \Lambda \mathcal{B}$), completing the link between the invariant, the Murray family, and the energetic balance at optimality.

C. Angle selection by junction translation

Let \mathbf{e}_i be unit vectors pointing outward along the three branches. An infinitesimal translation of the junction by $\delta \mathbf{x}$ changes the segment lengths as $\delta \ell_i = -\mathbf{e}_i \cdot \delta \mathbf{x}$. Stationarity of \mathcal{L} with respect to this translation requires $\sum_i (\partial \mathcal{L} / \partial \ell_i) \mathbf{e}_i = \mathbf{0}$. Using $\partial \mathcal{L} / \partial \ell_i = (8\mu / \pi) Q_i^2 r_i^{-4} + \Lambda c_i r_i^m$ and eliminating the hydraulic prefactor with the radius stationarity (6) collapses the balance to a *tariff-weighted vector closure*

$$\sum_{i=0}^2 c_i r_i^m \mathbf{e}_i = \mathbf{0}. \quad (9)$$

This is the EPIC analogue of the classical angle laws obtained from minimum-work arguments in vascular branching (cf.

Zamir’s optimality analysis [8]) and is formally identical to force balance at a three-junction (Plateau–Young construction [17]), with “bit-tensions” $a_i \equiv c_i r_i^m$.

Taking magnitudes in (9) shows that the three “bit-tensions”

$$a_i \equiv c_i r_i^m \quad (i = 0, 1, 2)$$

close a Euclidean triangle. The daughter opening angle θ_{12} therefore obeys the usual cosine relation

$$\cos \theta_{12} = \frac{a_0^2 - a_1^2 - a_2^2}{2 a_1 a_2}.$$

For homogeneous tariffs $c_0 = c_1 = c_2$ with nearly symmetric daughters $r_1 = r_2 \equiv r$, continuity together with (8) gives $r_0 = 2^{1/\alpha} r$. In this symmetric limit the vector closure reduces to

$$a_0 = 2 a_1 \cos\left(\frac{\theta_{12}}{2}\right),$$

so that

$$\cos\left(\frac{\theta_{12}}{2}\right) = \frac{a_0}{2 a_1} = \frac{c r_0^m}{2 c r^m} = \frac{(2^{1/\alpha} r)^m}{2 r^m} = 2^{\frac{m}{\alpha} - 1} = 2^{\frac{2m}{m+4} - 1} = 2^{\frac{m-4}{m+4}}.$$

Thus the parameter-free prediction can be written compactly as

$$\cos\left(\frac{\theta_{12}}{2}\right) = 2^{\frac{2m}{m+4} - 1} = 2^{\frac{m-4}{m+4}},$$

which yields $\theta_{12} \approx 74.93^\circ$ for $m=2$ (volume-priced) and $\theta_{12} \approx 97.44^\circ$ for $m=1$ (surface-priced). Notably, the closure (9) depends only on (m, c_i) and is *independent* of the hydraulic exponent n in a generalized dissipation law $P_{\text{flow}} \propto Q^2 r^{-n}$; angles are fixed entirely by structural pricing, not by rheology.

When local structural pricing blends surface and volume, with per-length bit-rate

$$\frac{\mathcal{B}_i}{\ell_i} = a r_i^2 + b r_i,$$

the same translation step yields a modified, testable closure with effective weights

$$\sum_{i=0}^2 (6a r_i^2 + 5b r_i) \mathbf{e}_i = \mathbf{0},$$

providing a distinctive “mixed-tariff fingerprint” for angle control in platforms where upkeep has both bulk (volume-like) and boundary (surface-like) components.

D. Generalizations & rheology (summary)

Two extensions leave the angle law unchanged and modify only the flow–radius scaling. First, if the per-length dissipation follows a generalized law $P_{\text{flow}} \propto Q^2 r^{-n}$ (Poiseuille $n=4$; slip or non-Newtonian cases admit $n \neq 4$ [18, 19]), the translation stationarity that produced the tariff-weighted vector closure,

$$\sum_i c_i r_i^m \mathbf{e}_i = \mathbf{0}, \quad (10)$$

is unaffected: the opening angles depend only on (m, c_i) , not on n . The radius stationarity, however, changes the local flow–radius slope to

$$Q \propto \sqrt{c} r^{\frac{m+n}{2}}, \quad \alpha = \frac{m+n}{2},$$

so that the Murray exponent reflects the upkeep scaling m and the hydraulic exponent n , while the angle selection remains purely “bit-tensional” via (10).

Second, if the apparent viscosity depends on radius, $\mu = \mu(r)$, the stationarity step at fixed Q yields the *exact* branchwise invariant

$$\frac{Q_i^2}{c_i r_i^{m+4}} = \frac{\pi m \Lambda}{8 [4 \mu(r_i) - r_i \mu'(r_i)]} \equiv \kappa_{\text{eff}}(r_i), \quad (11)$$

which reduces to the Poiseuille form when $\mu' \equiv 0$. Writing $D(r) \equiv 4\mu(r) - r\mu'(r)$, the exact local slope follows by logarithmic differentiation,

$$\alpha_{\text{eff}}(r) = \frac{d \ln Q}{d \ln r} = \frac{1}{2} \left[(m+4) - \frac{d}{d \ln r} \ln D(r) \right],$$

so any increase of $\mu(r)$ with r depresses α_{eff} below $(m+4)/2$, and any decrease elevates it. In the slow-variation limit, $D(r) = 4\mu(r)[1 - \xi(r)]$ with $|\xi| \ll 1$, this reduces to the convenient approximation

$$\alpha_{\text{eff}}(r) = \frac{m+4}{2} - \frac{1}{2} \frac{d \ln \mu}{d \ln r} + \mathcal{O}\left(\xi, \xi^2, \frac{d\xi}{d \ln r}\right),$$

which matches the observed Fåhræus–Lindqvist trends in microvascular rheology [14–16].

A second invariant packages geometry, tariff weights, and rheology into a branch-independent scalar. Using $\tau_w = 4\mu(r)Q/(\pi r^3)$ and (11),

$$\mathcal{S}_i \equiv \frac{\tau_{w,i}}{\sqrt{c_i}} \frac{\sqrt{4\mu(r_i) - r_i \mu'(r_i)}}{\mu(r_i)} r_i^{\frac{2-m}{2}} = \sqrt{\frac{2m\Lambda}{\pi}},$$

so (for equal c_i) constant μ implies constant wall shear when $m=2$ and constant $\tau_w r^{1/2}$ when $m=1$. This provides a direct, length-free stationarity check complementary to radius–flow scaling.

Finally, the Euler condition admits a coordinate-free diagnostic that requires no knowledge of Λ :

$$\mathcal{I}_i \equiv \frac{\partial P_{\text{flow}} / \partial r_i}{\partial \mathcal{B} / \partial r_i} = -\Lambda \quad (i = 0, 1, 2),$$

equivalently $Q_i^2 / (c_i r_i^{m+4})$ equal across branches (or $Q_i^2 / (c_i r_i^{m+4}) \rightarrow \kappa_{\text{eff}}(r_i)$ in the $\mu(r)$ case via (11)). When the informational tariff is uniform and admissible variations hold \mathcal{B} fixed, the EPIC program collapses to the classical minimum-pumping benchmark at fixed (Q_1, Q_2) , so that the rheological and hydraulic generalizations above slot into a single, unit-consistent accounting without altering the geometry selection principles (10).

V. GROWTH–CONE BOUND: RATE LIMITS FOR RELIABLE STRUCTURE

The EPIC ledger yields a real-time, unitful constraint on the creation of *reliably decodable, stably maintained distinctions* within any space–time control volume. At each instant, the achievable rate is throttled by the smaller of two budgets: an *interior* budget purchased from dissipation at the audited tariff (bits per second), and a *boundary* budget set by the reliably decodable information that can cross the causal surface. This two-sided constraint is the *growth–cone* bound. The few ingredients it rests on—nonequilibrium entropy production [4], an operational Landauer price [20], data-processing at the boundary [21], and a finite-blocklength refinement [22]—are stated here; the full proof appears in § [Methods: Proof of the Growth–cone bound](#).

To make this precise, fix a control volume $V \subset \mathbb{R}^3$ with (possibly time-dependent) boundary Σ_t and outward normal \mathbf{n} . The audit presumes three premises:

(A1) *Audit & tariff.* The effective energetic price per reliable bit is

$$\varepsilon_b(x, t) = \zeta(x, t) k_B T(x, t) \ln 2, \quad \zeta \geq 1,$$

with T the node-isothermal audit temperature; ε_b is obtained operationally (calibration in § [VIII](#)).

(A2) *Information share of dissipation.* A measurable density of reliably executed operations $\dot{I}_v(x, t)$ [bit s⁻¹ m⁻³] satisfies

$$\sigma_s^{(\text{info})}(x, t) \geq \frac{\varepsilon_b(x, t)}{T(x, t)} \dot{I}_v(x, t).$$

(A3) *Reliable boundary communication.* Across Σ_t , physical channels operated at blocklength n and error probability ϵ deliver an ϵ -reliable rate density $C_\epsilon(n; x, t)$ [bit s⁻¹ m⁻²].

Let $I(t) \equiv \int_V \iota(x, t) dV$ denote the stock of ϵ -reliable, stably maintained distinctions [bit] at the audit's resolution. By definition, this stock cannot grow faster than the rate of reliable operations supplied in the interior, $\dot{I}(t) \leq \int_V \dot{I}_v dV$. Using (A2) and the conversion $\Psi_b \equiv \sigma_s T / \varepsilon_b$ (power-priced throughput; cf. Eq. (23)), the interior budget reads

$$\dot{I}(t) \leq \int_V \frac{\sigma_s(x, t) T(x, t)}{\varepsilon_b(x, t)} dV = \int_V \Psi_b(x, t) dV,$$

i.e., each watt of dissipated power purchases at most ε_b^{-1} reliable bits per second, aggregated over V .

A complementary, communication-limited budget comes from the fact that any genuinely new, reliably decodable information must enter through the boundary Σ_t via physical channels operated at the target reliability. With the reliable rate density $C_\epsilon(n; x, t)$ on Σ_t , data-processing and the reliability specification (A3) imply

$$\dot{I}(t) \leq \int_{\Sigma_t} C_\epsilon(n; x, t) dA.$$

Both faces act simultaneously; the achievable rate is throttled by the smaller of the two. The resulting *growth–cone* bound is

$$\frac{d}{dt} \int_V \iota dV \leq \min \left\{ \int_V \Psi_b(x, t) dV, \int_{\Sigma_t} C_\epsilon(n; x, t) dA \right\}. \quad (12)$$

In a steady, isothermal node the interior face collapses to $\int_V \Psi_b dV = \int_V \sigma_s T dV / \varepsilon_b = P_{\text{flow}} / \varepsilon_b$, so that

$$\dot{I} \leq \min \left\{ \frac{P_{\text{flow}}}{\varepsilon_b}, \int_{\Sigma_t} C_\epsilon(n; x, t) dA \right\}.$$

Interpreted in informational units, the bound states that (i) at fixed tariff, each watt inside the domain can fund at most ε_b^{-1} reliable bits per second, and (ii) no more reliable bits per second can enter than the boundary can convey at the stated blocklength and error. Equality occurs only when the nonlimiting face is slack (e.g., boundary not rate-limiting if the interior face binds) and the limiting face operates reversibly at the audit's reliability; finite-time premiums, extra proofreading, idle duty cycles, or unseen channels strictly reduce the attainable rate.

When boundary signaling can be characterized by a per–use capacity C (bit/use) and dispersion V , operated at symbol rate $W(x, t)$ (use/s) across a channel density $\rho_{\text{ch}}(x, t)$ (m⁻²), the finite–blocklength normal approximation gives the ϵ -reliable *local* rate density

$$C_\epsilon(n; x, t) = \rho_{\text{ch}}(x, t) W(x, t) \left[C - \sqrt{V/n} Q^{-1}(\epsilon) \right]_+,$$

where Q^{-1} is the Gaussian tail inverse and $[\cdot]_+$ truncates at zero. The penalty term $\sqrt{V/n} Q^{-1}(\epsilon)$ quantifies the gap to asymptotic capacity at blocklength n and vanishes like $n^{-1/2}$; the prefactor $\rho_{\text{ch}} W$ converts per–use rates to per–area, per–time units. Integrating C_ϵ over Σ_t therefore returns a boundary budget in [bit s⁻¹], the same currency as the interior face $\int_V \Psi_b dV$. Substituting this expression into (12) cleanly exposes the trade: spatial regions where the margin $C - \sqrt{V/n} Q^{-1}(\epsilon)$ is small throttle growth at the boundary, whereas elsewhere the interior bit budget $\int_V \Psi_b dV$ (or $P_{\text{flow}} / \varepsilon_b$ in steady nodes) is the active limiter.

All quantities in (12) are operational and commensurate. The interior term $\Psi_b = \sigma_s T / \varepsilon_b$ prices power density [W m⁻³] into [bit m⁻³ s⁻¹] at the audited [J/bit] tariff, while the boundary term C_ϵ already lives in [bit s⁻¹ m⁻²], so its surface integral matches the interior's [bit s⁻¹] total. In this sense, the growth–cone is the domain–level counterpart of the node objective (5): interior entropy production and boundary signaling are brought onto a single ledger, allowing geometry and control to be assessed by their common return—reliable distinctions per energetic cost—under heterogeneous, space– and time–dependent operating conditions.

VI. PATH TO FALSIFIABILITY: HRF FIRST-TYPE CLOSURE AND AUDIT PROTOCOL

A. Data introduction

To place EPIC on a falsifiable footing, the High–Resolution Fundus (HRF) database is used as an illustrative yet stringent

testbed for the node–level angle law. The goal is not to audit tariffs or assert global optimality over entire trees, but to pose a narrow, testable question: when the upkeep exponent m is inferred solely from $\{r_0, r_1, r_2, \theta_{12}\}$ —i.e., without using any directional information—do real junctions satisfy tariff–weighted vector closure *using directions never involved in fitting m* ? An affirmative result constitutes a *first-type closure*: a necessary (though not sufficient) compatibility between EPIC and observed vascular geometry.

The analysis converts each image into analyzable geometry along a single path from pixels to node features (Fig. 1). After segmentation (Sato + Otsu in the figure variant [26, 27]), vessels are skeletonized to one pixel by parallel thinning [28], degree-3 pixel clusters are de-duplicated, and short-arc principal-component (PCA) tangents are fit on the three branches to estimate local directions. Radii are read from the Euclidean-distance transform along each branch at fixed offsets from the junction, with trimmed aggregation to suppress local artifacts [29]. Parent/daughter assignment follows a conservative rule that selects as parent the branch most opposed to the sum of the other two directions, cross-checked by swapping with the fatter daughter. Standard quality gates are applied uniformly: minimum branch length and radius, a minimum PCA singular-value ratio (SVD S_0/S_1) to suppress unstable tangents, and a gate on the daughter–daughter opening (*baseline defaults for Fig. 2*: $\theta_{12} \in [30^\circ, 150^\circ]$; PCA $S_0/S_1 \geq 1.20$; *minimum branch length $\ell \geq 25$ pixels*; *minimum radius $r \geq 2$ pixels*). Panel (b) of Fig. 1 visualizes the skeleton and tangents used to measure $\{r_0, r_1, r_2, \theta_{12}\}$; panel (c) renders the tariff split ($c_0:c_1:c_2$) at each junction (RGB), outlines strict/loose/fail quality control (QC) in green/orange/red, and marks bracket-edge m with a thin ring. The full implementation of this image-to-node pipeline (including segmentation settings, skeletonization parameters, QC gates, and per-node feature extraction) is available in the public *EPICproject* repository [30] (tag v2-arxiv).

B. HRF analysis: held-out vector closure

EPIC predicts a tariff-weighted vector-closure condition at a degree-3 junction,

$$r_0^m \mathbf{e}_0 + r_1^m \mathbf{e}_1 + r_2^m \mathbf{e}_2 = \mathbf{0},$$

which is quantified via the misclosure $R(m)$ in Eq. (13). The test is intentionally information–split. In the first stage, it is infer a single upkeep exponent m *from geometry alone*—using only $\{r_0, r_1, r_2, \theta_{12}\}$ —by solving the scalar angle law

$$r_0^{2m} = r_1^{2m} + r_2^{2m} + 2 \cos \theta_{12} r_1^m r_2^m$$

within a fixed bracket. If the residual changes sign over the bracket, bisection is applied; otherwise, a bounded one-dimensional search is performed to minimize the absolute residual

$$\left| r_0^{2m} - r_1^{2m} - r_2^{2m} - 2 \cos \theta_{12} r_1^m r_2^m \right|.$$

The analytic near-symmetric solution is admitted as a tie-breaker. Crucially, branch directions ($\mathbf{e}_0, \mathbf{e}_1, \mathbf{e}_2$) are *held out* of

this inversion. Only after m is fixed are those directions scored by the normalized closure residual

$$R(m) = \frac{\|r_0^m \mathbf{e}_0 + r_1^m \mathbf{e}_1 + r_2^m \mathbf{e}_2\|}{r_1^m + r_2^m}, \quad (13)$$

with preregistered gates at $R < 0.55$ (strict) and $R < 0.85$ (loose). This separation prevents directional leakage: if directions had influenced the inversion, they would not reduce the held-out $R(m)$. The tariff split ($c_0:c_1:c_2$) shown in Fig. 1c is recovered from the nullspace of $[\mathbf{e}_0 \ \mathbf{e}_1 \ \mathbf{e}_2] \text{diag}(r_0^m, r_1^m, r_2^m)$ *for visualization only*; it is not used to fit m or to score $R(m)$. All residuals, null distributions, and bootstrap summaries reported in Figs. 2 and 3 are produced by the analysis scripts in the EPICproject repository [30].

On HRF with the Sato + Otsu segmentation ($N = 19,127$ junctions), strict and loose QC acceptance rates are 89.7% and 98.1%, respectively. The per-node upkeep exponent has median $m_{\text{med}} = 0.784$ with interquartile range $m \in [0.200, 1.416]$. The held-out closure residuals $R(m)$ (column R_{m_holdout}) have median $\tilde{R} = 0.213$ with bootstrap 95% CI $[0.209, 0.217]$, and 6160/19,127 nodes ($\approx 32.2\%$) lie within ± 0.02 of the m -bracket edges. Parent assignment under the geometric opposition rule is flagged as ambiguous in 84.8% of nodes, with potential leakage controlled by held-out scoring and daughter-swap nulls. The preregistered held-out test (PREREG_C1) reports $\tilde{R} = 0.2129$ with bootstrapped 95% CI $[0.2089, 0.2166]$, worst one-sided $p_{\text{med}} = p_{\text{frac}} = 2.0 \times 10^{-4}$, and max Cliff's $\delta = -0.84$. The comparison in Fig. 2 then contrasts real junctions with four structure-preserving counterfactuals: (i) shuffled directions within image, (ii) swapped daughters, (iii) randomized daughter bearings at fixed θ_{12} , and (iv) shuffled radii within image. The observed $R(m)$ histogram lies well to the left of every null, and the bootstrap median (solid line) remains comfortably below the strict gate (95% bootstrap CI [31]). To probe measurement stability, 10% independent Gaussian jitter is applied to the radii followed by re-inversion of m per node from $\{r_0, r_1, r_2, \theta_{12}\}$; the dotted median in Fig. 2 is essentially unchanged under this perturbation.

To exclude artifacts from quality-control parameters, an ablation varying the two dominant geometry gates—the minimum daughter–daughter angle and the minimum PCA singular-value ratio—shows the median $R(m)$ tightly clustered at ≈ 0.203 – 0.210 across the grid (Fig. 3), well below the strict threshold 0.55. Thus, neither a laxer angle gate nor a stricter tangent criterion drives the effect. Taken together with the null controls, this supports a *first-type closure*: with m inferred from $\{r_0, r_1, r_2, \theta_{12}\}$ alone, real HRF junctions close on held-out directions substantially better than strong structure-preserving counterfactuals, and the separation is robust to radius noise and QC scans. Scope remains local and geometric at degree-3 junctions; this is not yet a tariff audit, a rheological fit, or a claim of global optimality.

C. Future steps: audit protocol and transportability

A concise path to falsifiability follows. (1) *Weighted vs. unweighted Murray*: compute $D_\alpha = |r_0^\alpha - r_1^\alpha - r_2^\alpha|$ with

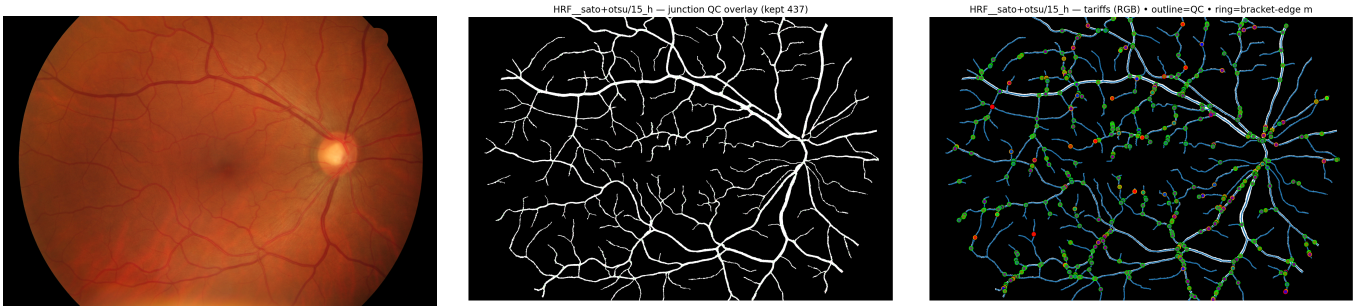


FIG. 1. **From image to analyzable geometry (HRF).** (a) Original fundus image (HRF, file 15_h), reproduced from the High-Resolution Fundus (HRF) Image Database (Pattern Recognition Lab, FAU), [CC BY 4.0](#) [23]. Changes: downsampling for layout; overlays in (b,c) added. When HRF is used to evaluate methods, cite Budai *et al.* (IJoBI 2013) [24]; when segmentation labels are used, cite Odstrčilík *et al.* (IET Image Processing 2013) [25].

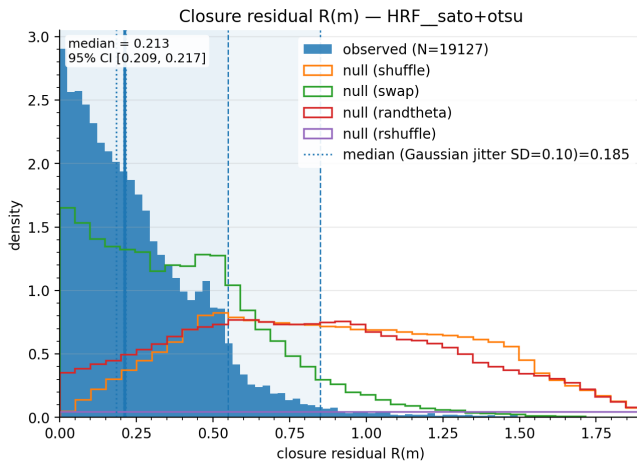


FIG. 2. **Held-out closure residuals on HRF (Sato + Otsu).** Histogram of $R(m)$ from (13) over all HRF junctions (blue; $N=19,127$); solid line: observed median with 95% bootstrap CI [31]; dotted line: median under 10% radius jitter with re-inversion of m . Colored outlines: structure-preserving nulls: *shuffle* (shuffle directions within image), *swap* (swap daughters), *randtheta* (randomize daughter bearings at fixed θ_{12}), and *rshuffle* (shuffle radii within image). The observed distribution lies well to the left of all nulls; lower is better. Shaded bands indicate preregistered strict/loose thresholds.

$\alpha = (m + 4)/2$ from angle-only inversion, then score on held-out $\|\sum_i r_i^m \mathbf{e}_i\|$; require superiority to all four nulls on both the median and $\Pr[R < 0.55]$ with one-sided $p \leq 10^{-3}$ and Cliff's δ [32] ≤ -0.20 . (2) *Near-symmetric angle law*: compare the θ_{12} distribution at $r_1 \approx r_2$ to the analytic EPIC curve; accept if bin-wise medians and CIs track the prediction (e.g., 74.93° for $m=2$, 97.44° for $m=1$) within preregistered tolerances; for historical context on unweighted Murray baselines see [33]. (3) *Parent-direction prediction*: verify that the EPIC vector sum identifies the parent more accurately than fixed- m baselines ($m=2$, $m=1$, equal-weight 120°), with paired sign-tests on the per-node angle error ϕ_0 meeting $\alpha \leq 10^{-4}$ [34]. (4) *Priced-shear invariant*: under locally constant viscosity, require branch-independent wall shear for $m=2$ (or invariance of $\tau_w r^{1/2}$ for $m=1$) and contraction of within-node variance relative to

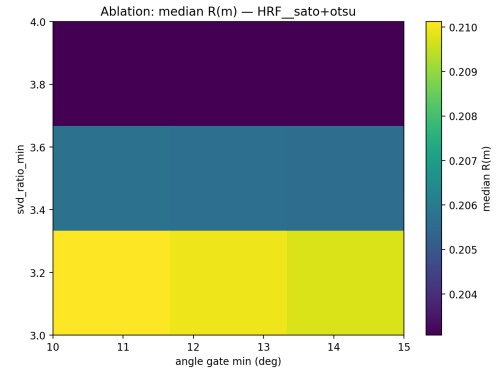


FIG. 3. **Ablation of held-out closure (HRF, Sato + Otsu).** Median $R(m)$ (color scale) as a function of the lower bound on θ_{12} and the minimum PCA singular-value ratio for tangent acceptance. All cells fall in a narrow band $R(m) \approx 0.203\text{--}0.210$, far below the strict threshold 0.55, indicating stability to QC gating.

radius-shuffle controls. (5) *Power split audit*: in systems with metered structure and flow, test $nP_{\text{flow}} = mP_{\text{struct}}$ with confidence intervals excluding large deviations.

Additionally, the design-level predictions developed in §VII admit targeted, stringent tests that move beyond angle-only closure:

(6) *EPIC optics (Snell-type refraction)*. In phantoms or tissues engineered with a known step in the price field $[\varepsilon_{bc}]$, test the refraction law $n_1 \sin \theta_1 = n_2 \sin \theta_2$ (Eq. (20)). Normalize by independently estimated n_i and fit a constrained line; *accept* if the slope's 95% CI spans unity and rotated/shuffled nulls are strongly rejected (one-sided $p \leq 10^{-3}$).

(7) *Scale-out and transportability*. Replicate on DRIVE, STARE, and CHASE_DB1 [35–37] under a frozen preregistration (fixed tangent length, SVD threshold, angle gates, segmentation strata). Require: (i) the held-out $R(m)$ distribution remains left-shifted relative to the within-image shuffle null ($p \leq 10^{-3}$); (ii) in the near-symmetric regime, the share within $|\Delta m| \leq 0.25$ is $\geq 70\%$ and the Theil–Sen slope CI includes 1 [38, 39]; (iii) vessel-size stratification yields $\alpha_{\text{eff}}(r)$ consistent with $Q \propto r^{(m+n)/2}$ within reported CIs.

(8) *Per-node uncertainty*. Report radius-jitter and

tangent-noise ensembles; *accept* if the median 95% half-width for m is ≤ 0.35 and $\geq 60\%$ of bracket-edge nodes move off-edge under uncertainty. For independent falsification and reproducibility, release node-level CSVs (radii, angles, m , $R(m)$, QC flags), the exact segmentation variants, and a concise preregistration that fixes all degrees of freedom before scoring.

Beyond the retina, the same held-out closure and near-symmetric angle tests apply to brain, kidney, and tumor microvasculature (abundant degree-3 nodes; heterogeneous $\mu(r)$); to pulmonary and bronchial trees (symmetric-angle predictions and local power splits testable against morphometry and pressure–flow); to lymphatic networks (mixed-tariff fingerprints in the vector closure); and to plant xylem/phloem and engineered microfluidics (EPIC optics under designed tariff gradients). Across these settings the criterion is uniform: infer m from geometry alone, score on genuinely held-out directions, confront structure-preserving nulls under preregistered thresholds, and publish the full node-level ledger to enable reproduction—or refutation—of every statistic reported in Figs. 1–3.

VII. DESIGN COROLLARIES AND BROADER IMPLICATIONS (“EPIC OPTICS”)

This section moves from node-level closure to *design-level* consequences of the EPIC ledger, $\mathcal{L} = P_{\text{flow}} + \Lambda \mathcal{B}$, where P_{flow} accounts for hydraulic dissipation and $\Lambda \mathcal{B}$ prices structure. The only ingredients used are the homogeneities of transport ($P_{\text{flow},i} \propto Q_i^2 r_i^{-n}$) and structure ($\mathcal{B}_i \propto r_i^m$); no calibration of Λ or additional constitutive detail is required. From these homogeneities, stationarity with respect to (i) translations and (ii) dilations yields compact rules that are independent of network topology and boundary conditions and therefore suitable both for analysis and for engineering use.

Three corollaries follow and are developed below. **(A) Equipartition under dilation.** A uniform infinitesimal dilation of all radii enforces a universal split of power between flow and structure, $nP_{\text{flow}} = mP_{\text{struct}}$ (Eq. (14)), which fixes the fractions $P_{\text{flow}}/(P_{\text{flow}} + P_{\text{struct}}) = m/(m+n)$ and $P_{\text{struct}}/(P_{\text{flow}} + P_{\text{struct}}) = n/(m+n)$ irrespective of demands or lengths. **(B) Concave effective edge cost.** Eliminating radii at the stationary point yields an effective per-length cost $\propto [\varepsilon_b(x)c(x)]^{n/(m+n)} Q^{2m/(m+n)}$ (Eq. (17)); the exponent $\gamma = 2m/(m+n) \in (0, 2)$ is strictly concave in the regimes of interest (Eq. (18)), implying that merging flows into shared trunks is generically cheaper than routing them in isolation and thus explaining the prevalence and depth of tree-like hierarchies. **(C) Routing index and refraction.** Factoring the spatially varying price field defines an *EPIC index* $n(x) \propto [\varepsilon_b(x)c(x)]^{n/(m+n)}$ that turns path optimization into an “optical path length” problem; its gradients bend optimal routes toward cheaper regions, and across sharp price jumps the stationary path obeys a Snell-type refraction law $n_1 \sin \theta_1 = n_2 \sin \theta_2$ (Eq. (20)).

Taken together, these results constitute a geometrical-optics calculus for tariffed media. They (i) predict how power budgets partition under scaling, (ii) explain why branching architectures dominate and how their depth shifts with (m, n) , and (iii) provide a quantitative index for routing in heterogeneous

“price fields” $\varepsilon_b(x)c(x)$. The subsections that follow present these corollaries in turn—deriving the relations, stating their assumptions explicitly, and articulating the empirical tests they motivate.

A. Equipartition under dilation (universal power split)

Assume a per-length transport law $P_{\text{flow},i} = \kappa_i Q_i^2 r_i^{-n}$ with $n > 0$ (Poiseuille $n=4$ for Newtonian laminar tubes; other n capture slip or non-Newtonian regimes) and a structural pricing law $\mathcal{B}_i = \beta_i r_i^m$ with $m > 0$ (volume-priced $m=2$, surface-priced $m=1$, or a calibrated mix) [10, 11, 18]. The positive coefficients κ_i, β_i may absorb segment length and material factors but do not depend on r_i . With exogenous demands Q_i and topology held fixed, the EPIC ledger reads

$$\mathcal{L}(\{r_i\}) = \sum_i \kappa_i Q_i^2 r_i^{-n} + \Lambda \sum_i \beta_i r_i^m \equiv P_{\text{flow}} + P_{\text{struct}},$$

and an interior optimum is considered (all $r_i > 0$ with no active bounds).

A uniform infinitesimal dilation $r_i \mapsto (1+\epsilon)r_i$ provides an admissible first-order variation. By the chain rule,

$$\begin{aligned} \left. \frac{d\mathcal{L}}{d\epsilon} \right|_{\epsilon=0} &= \sum_i r_i \frac{\partial \mathcal{L}}{\partial r_i} \\ &= \sum_i \left[r_i \frac{\partial}{\partial r_i} (\kappa_i Q_i^2 r_i^{-n}) + r_i \frac{\partial}{\partial r_i} (\Lambda \beta_i r_i^m) \right]. \end{aligned}$$

The two derivatives in the brackets are elementary. Since

$$\frac{\partial}{\partial r_i} (\kappa_i Q_i^2 r_i^{-n}) = -n \kappa_i Q_i^2 r_i^{-n-1},$$

$$\frac{\partial}{\partial r_i} (\Lambda \beta_i r_i^m) = m \Lambda \beta_i r_i^{m-1},$$

multiplying each by r_i gives

$$r_i \frac{\partial}{\partial r_i} (\kappa_i Q_i^2 r_i^{-n}) = -n \kappa_i Q_i^2 r_i^{-n},$$

$$r_i \frac{\partial}{\partial r_i} (\Lambda \beta_i r_i^m) = m \Lambda \beta_i r_i^m.$$

Substituting these into the expression for $d\mathcal{L}/d\epsilon$ yields

$$\begin{aligned} \left. \frac{d\mathcal{L}}{d\epsilon} \right|_{\epsilon=0} &= \sum_i [-n \kappa_i Q_i^2 r_i^{-n} + m \Lambda \beta_i r_i^m] \\ &= -n \sum_i \kappa_i Q_i^2 r_i^{-n} + m \Lambda \sum_i \beta_i r_i^m \\ &= -n P_{\text{flow}} + m P_{\text{struct}}, \end{aligned}$$

where $P_{\text{flow}} \equiv \sum_i \kappa_i Q_i^2 r_i^{-n}$ and $P_{\text{struct}} \equiv \Lambda \sum_i \beta_i r_i^m$.

First-order optimality requires the directional derivative to vanish for every admissible direction; in particular, the dilation direction imposes

$$n P_{\text{flow}} = m P_{\text{struct}}, \quad P_{\text{struct}} \equiv \Lambda \mathcal{B} = \Lambda \sum_i \beta_i r_i^m. \quad (14)$$

This equipartition relation depends only on the homogeneity exponents (m, n) and standard unconstrained optimality conditions [40, 41].

The same conclusion follows edgewise from stationarity. Setting $\partial \mathcal{L} / \partial r_i = 0$ gives

$$\begin{aligned} -n \kappa_i Q_i^2 r_i^{-n-1} + m \Lambda \beta_i r_i^{m-1} &= 0, \\ n \kappa_i Q_i^2 r_i^{-n} &= m \Lambda \beta_i r_i^m \quad (\forall i). \end{aligned}$$

so transport and structure are locally balanced on every free edge; summing over i recovers (14). Solving the per-edge condition for r_i yields the closed-form scaling

$$r_i^{m+n} = \frac{n \kappa_i}{m \Lambda \beta_i} Q_i^2 \implies r_i \propto \Lambda^{-1/(m+n)} Q_i^{2/(m+n)}.$$

A global tariff rescaling $\Lambda \mapsto a \Lambda$ therefore multiplies all optimal radii by the common factor $a^{-1/(m+n)}$ while leaving the fractional power shares unchanged by (14). Because branching angles arise from translation stationarity (cf. Eq. (9)) and are independent of Λ , the angle geometry is likewise invariant under tariff rescaling.

The physical content is transparent: the homogeneity exponents (m, n) alone set how an optimal network allocates its power budget between transport and structure. In the canonical Newtonian/volume case $(n, m) = (4, 2)$ one obtains $P_{\text{flow}} : P_{\text{struct}} = 1 : 2$; for Newtonian/surface $(4, 1)$ the split is $1 : 4$, consistent with classical minimum-work heuristics [5, 7, 8]. These ratios furnish sharp audit targets: systematic deviations indicate active constraints (violating the interior assumption), departures from the assumed homogeneities (e.g., radius-dependent effective n from Fåhræus–Lindqvist and shear-thinning), or operation away from stationarity [14–16].

B. Concavity of the effective edge cost and the prevalence of trees

At a fixed location x , consider a single conduit of radius r that carries flow Q through a medium with local tariff $\varepsilon_b(x)c(x)$. Under the same homogeneity assumptions as above, the per-length contribution of that conduit to the EPIC ledger can be written (up to geometry-independent constants) as

$$\ell(Q, r; x) = \kappa(x) Q^2 r^{-n} + \Lambda \beta(x) r^m,$$

with $n > 0$, $m > 0$, and $\kappa(x), \beta(x) > 0$. Here $\kappa(x)$ encodes the local hydraulic law (viscosity, length, roughness), while $\beta(x)$ collects the local structural bit-density and duty cycle; $\Lambda = \lambda \varepsilon_b$ prices each structural bit in J/bit. The first term is the per-length pumping cost and the second is the priced upkeep cost for keeping the conduit present and functional, in the spirit of Murray-type minimum-work optimizations of vascular trees [5, 8].

For fixed Q and x , the optimal radius $r^*(Q; x)$ minimizes $\ell(Q, r; x)$ subject to $r > 0$. Stationarity gives

$$\frac{\partial \ell}{\partial r} = -n \kappa(x) Q^2 r^{-n-1} + m \Lambda \beta(x) r^{m-1} = 0,$$

so at optimality

$$n \kappa(x) Q^2 r^*(Q; x)^{-n} = m \Lambda \beta(x) r^*(Q; x)^m. \quad (15)$$

Solving (15) for the optimal radius yields

$$\begin{aligned} r^*(Q; x)^{m+n} &= \frac{n \kappa(x)}{m \Lambda \beta(x)} Q^2, \\ r^*(Q; x) &\propto [\Lambda \beta(x)]^{-1/(m+n)} Q^{2/(m+n)}. \end{aligned} \quad (16)$$

Substituting r^* back into ℓ and using (15) to eliminate one of the two terms gives the optimal per-length cost

$$\begin{aligned} \ell^*(Q; x) &\equiv \ell(Q, r^*(Q; x); x) = \frac{m+n}{m} \Lambda \beta(x) r^*(Q; x)^m \\ &= \frac{m+n}{n} \kappa(x) Q^2 r^*(Q; x)^{-n}. \end{aligned}$$

Using the scaling from (16),

$$r^*(Q; x)^m \propto \kappa(x)^{\frac{m}{m+n}} [\Lambda \beta(x)]^{-\frac{m}{m+n}} Q^{\frac{2m}{m+n}},$$

one obtains

$$\ell^*(Q; x) \propto [\Lambda \beta(x)]^{\frac{n}{m+n}} \kappa(x)^{\frac{m}{m+n}} Q^{\frac{2m}{m+n}}. \quad (17)$$

The prefactor $\kappa(x)^{m/(m+n)}$ encodes purely hydraulic information (e.g., local viscosity and length), while $\Lambda \beta(x)$ carries the information tariff. Writing $\Lambda = \lambda \varepsilon_b$ and $\beta(x) \propto c(x)$ shows that, up to a geometry-independent constant,

$$\ell^*(Q; x) \propto [\varepsilon_b(x) c(x)]^{\frac{n}{m+n}} Q^\gamma, \quad \gamma \equiv \frac{2m}{m+n},$$

which is the effective per-length cost density advertised in Eq. (17).

The exponent

$$\gamma = \frac{2m}{m+n} \quad (18)$$

lies in $(0, 2)$ for any $m, n > 0$, and in the regimes of interest $m < n$ (e.g., Poiseuille flow with $n = 4$ and structural pricing dominated by $m \in \{1, 2\}$) one has $0 < \gamma < 1$. On $(0, \infty)$ the map $Q \mapsto Q^\gamma$ is then strictly concave: $f'(Q) = \gamma Q^{\gamma-1} > 0$ and

$$f''(Q) = \gamma(\gamma-1) Q^{\gamma-2} < 0 \quad (Q > 0, 0 < \gamma < 1),$$

so in particular

$$(Q_1 + Q_2)^\gamma < Q_1^\gamma + Q_2^\gamma \quad \text{for all } Q_1, Q_2 > 0, 0 < \gamma < 1.$$

Because $\ell^*(Q; x)$ differs from Q^γ only by a positive multiplicative factor, the same strict subadditivity holds for the optimal edge cost. For two positive demands Q_1, Q_2 at fixed x ,

$$\ell^*(Q_1 + Q_2; x) < \ell^*(Q_1; x) + \ell^*(Q_2; x) \quad (0 < \gamma < 1),$$

so routing both flows through a shared trunk is cheaper than carrying them on two isolated edges. In other words, concavity of the optimal edge cost makes *trees energetically preferred*: mergers reduce the per-length cost.

The strength of the concavity, controlled by γ , has immediate architectural implications. Smaller γ (more concave cost; e.g.,

surface-priced upkeep with $m=1$ or reduced n from slip or shear-thinning) makes early mergers energetically favorable and drives thicker trunks upstream, while larger γ (less concave cost) delays mergers and yields shallower hierarchies. Thus measured shifts in the exponents (m, n) translate directly into systematic changes in branching depth and load sharing, even before any specific material parameters are specified. This picture aligns with constructal arguments for tree-shaped flow architectures [13, 42] and with optimality analyses of arterial branching [8], providing a quantitative, tariff-aware version of the intuition that “branching pays” when the effective transport cost is a concave function of flux.

C. Routing index and Snell-like refraction (“EPIC optics”)

The effective edge cost (17) cleanly separates the dependence on flow from the dependence on the local price field. For a conduit segment at position x carrying a prescribed flux Q , the optimal per-length cost takes the form

$$\ell^*(Q; x) \propto [\varepsilon_b(x) c(x)]^{\frac{n}{m+n}} Q^\gamma, \quad \gamma = \frac{2m}{m+n},$$

so that, along any path where Q is fixed, the only spatially varying factor is

$$\mathfrak{n}(x) \propto [\varepsilon_b(x) c(x)]^{\frac{n}{m+n}}.$$

This quantity is referred to as the *EPIC index*. For a path Γ connecting two points, parameterized by arclength s , the total priced cost is therefore

$$\mathcal{J}[\Gamma] \propto \int_{\Gamma} \ell^*(Q; x) ds \propto Q^\gamma \int_{\Gamma} \mathfrak{n}(x) ds,$$

and minimizing cost at fixed Q is equivalent to minimizing the “optical path length”

$$\mathcal{S}[\Gamma] \equiv \int_{\Gamma} \mathfrak{n}(x) ds, \quad (19)$$

exactly as in geometric optics, where rays minimize $\int n(x) ds$ in a medium of refractive index $n(x)$ [43, 44].

Two standard consequences of (19) are particularly transparent in EPIC form. First, consider a sharp interface separating two regions with constant indices \mathfrak{n}_1 and \mathfrak{n}_2 . The crossing point of the path with the interface is allowed to vary, while endpoints are held fixed. Stationarity of \mathcal{S} with respect to that crossing point yields the familiar Snell-type condition

$$\mathfrak{n}_1 \sin \theta_1 = \mathfrak{n}_2 \sin \theta_2, \quad (20)$$

where θ_i is the angle between the path and the interface normal in region i [43]. Entering a cheaper region (smaller \mathfrak{n}) the stationary path bends away from the normal, spending more arclength in the low-tariff side; entering a more expensive region it bends toward the normal. When $\mathfrak{n}_1 > \mathfrak{n}_2$ and $\sin \theta_1 > \mathfrak{n}_2/\mathfrak{n}_1$, no transmitted stationary path exists and the path undergoes “total internal reflection” at the interface: leaving the cheap corridor would be too costly in the EPIC currency.

Second, when $\mathfrak{n}(x)$ varies smoothly, the Euler–Lagrange equations for the functional (19) give the ray equation

$$\frac{d}{ds} (\mathfrak{n} \hat{\mathbf{t}}) = \nabla_{\perp} \mathfrak{n},$$

where $\hat{\mathbf{t}}$ is the unit tangent to the path and ∇_{\perp} denotes the component of $\nabla \mathfrak{n}$ perpendicular to $\hat{\mathbf{t}}$ [43, 44]. The left-hand side is the curvature vector of the path scaled by \mathfrak{n} , while the right-hand side points toward decreasing \mathfrak{n} . Optimal routes therefore curve toward cheaper tariff, and in media where $\varepsilon_b(x)$ or $c(x)$ varies anisotropically (for example through spatially structured control burdens or upkeep densities), the resulting conduits “hug” corridors of low $\mathfrak{n}(x)$. At the network scale this produces systematic anisotropies and funneling effects that can be read directly from maps of $\mathfrak{n}(x)$.

These observations turn heterogeneity in the price field into a measurable object. Because $\mathfrak{n}(x) \propto [\varepsilon_b(x) c(x)]^{n/(m+n)}$, any independent estimate of the energetic tariff $\varepsilon_b(x)$ (audit-level J/bit) and structural coefficient $c(x)$ (bit-density per geometry) converts an observed routing pattern into a quantitative $\mathfrak{n}(x)$ map. Conversely, in settings where direct audits are infeasible, geometry alone constrains *ratios* of local tariffs: the Snell relation (20) fixes $\mathfrak{n}_2/\mathfrak{n}_1$ across sharp transitions, and curvature of optimal paths constrains gradients of $\mathfrak{n}(x)$. In both regimes the refraction signatures implied by (19) provide sharp, falsifiable predictions for how spatial variations in $[\varepsilon_b c]$ imprint themselves on conduit geometry.

Summary. The three ingredients above are purely kinematic consequences of the EPIC ledger together with the homogeneities of transport and structural pricing. First, a uniform dilation fixes a *universal* power split $nP_{\text{flow}} = mP_{\text{struct}}$ (Eq. (14)), so the fractions $P_{\text{flow}}/(P_{\text{flow}} + P_{\text{struct}})$ and $P_{\text{struct}}/(P_{\text{flow}} + P_{\text{struct}})$ depend only on (m, n) , not on geometry or load. Second, eliminating radii at stationarity yields a concave edge cost with exponent $\gamma = 2m/(m+n)$ (Eq. (18)), which makes mergers energetically favorable and explains why branching architectures proliferate and how their depth shifts when (m, n) change. Third, the routing index $\mathfrak{n}(x) \propto [\varepsilon_b(x) c(x)]^{n/(m+n)}$ turns spatial heterogeneity of $[\varepsilon_b c]$ into measurable refraction (Eqs. (17)–(20)), so that optimal paths bend toward cheaper regions in a Snell-like fashion. Taken together, these “EPIC optics” rules link morphology directly to audited tariffs and geometry: they predict how radii rescale with price, how branching hierarchies reorganize under altered upkeep and rheology, and how routing patterns in heterogeneous media encode the underlying price field in units that connect cleanly to operational audits (J/bit) and physical dimensions (m).

VIII. CONCLUSION

EPIC changes the accounting, not the physics. The transport laws remain classical; what changes is the currency in which structure is priced. By auditing a node’s control layer in absolute units (J/bit), EPIC converts entropy production into a spendable, unitful budget for maintaining reliable distinctions

and selects geometry by a single, constrained ledger,

$$\mathcal{L} = P_{\text{flow}} + \Lambda \mathcal{B}, \quad \Lambda = \lambda \varepsilon_b, \quad \varepsilon_b = \zeta k_B T \ln 2.$$

From this priced extremum one obtains three “hard” geometric outputs that put Murray’s picture on measurable rails. **(i) Weighted Murray.** The stationarity invariant equalizes $Q_i^2/(c_i r_i^{m+4})$ across branches, yielding

$$Q \propto r^\alpha, \quad \alpha = \frac{m+4}{2}, \quad \Rightarrow \quad \sqrt{c_0} r_0^\alpha = \sqrt{c_1} r_1^\alpha + \sqrt{c_2} r_2^\alpha,$$

which recovers the cubic law when upkeep is volume-priced ($m=2 \Rightarrow \alpha=3$) and its surface-priced counterpart when wall burden dominates ($m=1 \Rightarrow \alpha=2.5$); with general hydraulic exponent n this local slope is $\alpha_{\text{eff}} = \frac{m+n}{2}$, accommodating rheological departures without altering first principles. **(ii) Angle closure.** Translating the junction eliminates material prefactors and fixes the directions by a tariff-weighted vector law,

$$\sum_{i=0}^2 c_i r_i^m \mathbf{e}_i = \mathbf{0},$$

which predicts near-symmetric daughter angles of $\approx 75^\circ$ for $m=2$ and $\approx 98^\circ$ for $m=1$ under homogeneous tariffs, and supplies a distinct mixed-tariff fingerprint when surface and volume contributions blend. **(iii) Growth-rate bound.** At any audit, the rate of creating stably maintained, reliably decodable distinctions is throttled by a two-faced *growth-cone*: the *interior* bit budget purchasable from dissipation at the audited tariff, $\int_V \Psi_b dV = P_{\text{flow}}/\varepsilon_b$, and the *boundary* reliable throughput across the causal surface; the achievable \dot{I} is the minimum of the two.

Beyond these node laws, three design rules “set in stone” how morphology responds to prices. **Equipartition (dilation).** Homogeneity alone enforces $nP_{\text{flow}} = mP_{\text{struct}}$, so the optimal power split is universal, radii rescale as $r \propto (\Lambda c)^{-1/(m+n)}$ at fixed demands, and angles are unchanged. **Concavity.** Eliminating r along an edge yields an effective per-length cost $\propto [\varepsilon_b c]^{n/m+n} Q^\gamma$ with $\gamma = \frac{2m}{m+n}$: for the common $m < n$ regime (e.g., Poiseuille with $m=1$ or 2) this is strictly concave ($\gamma < 1$), so merging flows is cheaper than isolating them—trees proliferate—and the branching depth shifts predictably with upkeep mix (m) and rheology (n). **Refraction (EPIC optics).** The same elimination defines an *EPIC index* $n(x) \propto [\varepsilon_b(x)c(x)]^{n/m+n}$; optimal routes minimize $\int n ds$ and obey a Snell-like law $n_1 \sin \theta_1 = n_2 \sin \theta_2$, bending toward cheaper-tariff corridors. **Unitful, falsifiable, design-ready.** Every statement above is unit bearing (J/bit, W, m) and admits preregistered tests: weighted-vs-unweighted Murray residuals; angle predictions and vector-closure with held-out directions; near-symmetric angle drift under controlled surface/volume perturbations; and refraction across engineered tariff jumps. The priorities are clear: (1) audit ε_b and c with uncertainties; (2) probe the surface–volume mix to move α and the symmetric angle in the predicted directions; (3) map $n(x)$ to forecast routing in heterogeneous media; and (4) identify when the boundary face—not the interior budget—limits \dot{I} . In short, EPIC supplies

a calibrated ledger (J/bit) that *prices* structure, restores Murray’s law as a special case, fixes angles, bounds growth, and furnishes simple design rules (equipartition, concavity, refraction) that make morphology calculable and testable in the laboratory.

NOTATION AND UNITS (QUICK REFERENCE)

- Q : Volumetric flow rate — m^3/s . Segment-level demand (fixed daughters).
 r, ℓ : Segment radius, length — m. Long-tube (Poiseuille) assumption.
 μ : Dynamic viscosity — Pa s. May depend on r in microvasculature.
 Δp : Pressure drop — Pa. Per segment.
 P_{flow} : Hydraulic (dissipated) power — W. $\sum_i Q_i \Delta p_i$.
 σ_s : Entropy-production density — W/(K m^3). Local, non-negative.
 T : Temperature — K. Isothermal within a node.
 Ψ_b : Information throughput density — bit/($\text{m}^3 \text{s}$). $\Psi_b = \sigma_s T / \varepsilon_b$.
 ε_b : Effective bit energy — J/bit. $\varepsilon_b = \zeta k_B T \ln 2$.
 ζ : Overhead factor — dimensionless. $\zeta \geq 1$ (reliability, refresh, control).
 β : Bit-rate density — bit/($\text{m}^3 \text{s}$). Audit-level rate of reliable ops.
 \mathcal{B} : Structural bit-rate (node) — bit/s. $\sum_i c_i \ell_i r_i^m$.
 c_i : Tariff coefficient — bit/s $\text{m}^{-(m+1)}$. In $\mathcal{B}_i = c_i \ell_i r_i^m$.
 m : Upkeep exponent — dimensionless. $m=2$ (volume), $m=1$ (surface).
 n : Hydraulic exponent — dimensionless. Poiseuille $n=4$ (other n for slip/non-Newtonian).
 Λ : Priced-bit multiplier — J/bit. $\Lambda = \lambda \varepsilon_b$.
 κ : Stationarity invariant — $\text{m}^3/\text{s/bit}$. $Q_i^2/(c_i r_i^{m+4})$.
 τ_w : Wall shear stress — Pa. $4\mu Q/(\pi r^3)$ (laminar).
 \dot{S}_{tot} : Total entropy-production rate — W/K. $\int_V \sigma_s dV$.
 P_{diss} : Dissipated power (domain) — W. $\int_V \sigma_s T dV$.
 I, \dot{I} : Stored distinctions; creation rate — bit, bit/s. At audit reliability.
 η_b : Structural information efficiency — bit/J. $\eta_b = \varepsilon_b^{-1}$.
 θ : Junction angle — $^\circ$. Between branch axes.
Note: 1 nat = $\ln 2$ bits; convert via nat = bit $\times \ln 2$.

METHODS: CALIBRATION AND RELIABILITY

Audit window and effective bit energy. Fix an audit window of duration $\tau > 0$ and a node-isothermal audit temperature T . Let $\langle P_{\text{ctrl}} \rangle_\tau$ denote the *baseline-subtracted* mean power of the control/housekeeping layer over $[t_0, t_0 + \tau]$, and let $\langle \dot{I}_{\text{rel}} \rangle_\tau$ be the mean *reliably decodable* bit-rate (at the declared error target) over the same window. The (operational) energetic tariff per reliable bit and its Landauer-normalized overhead are

$$\varepsilon_b = \frac{\langle P_{\text{ctrl}} \rangle_\tau}{\langle \dot{I}_{\text{rel}} \rangle_\tau} \quad [\text{J bit}^{-1}], \quad (21)$$

$$\zeta \equiv \frac{\varepsilon_b}{k_B T \ln 2} \geq 1. \quad (22)$$

Reliability normalization. If reliability is specified as a symbol (bit) error $p_e \in [0, \frac{1}{2})$, the reliably decodable fraction per raw bit equals $1 - H_b(p_e)/\ln 2$, where

$$H_b(p) = -p \ln p - (1-p) \ln(1-p)$$

is the binary entropy (nats). The corresponding reliability multiplier is

$$\zeta_{\text{rel}} = [1 - H_b(p_e)/\ln 2]^{-1} \geq 1.$$

Factorization of overheads. The audit multiplier ζ is dimensionless and factorizable:

$$\zeta = \zeta_{\text{speed}} \zeta_{\text{rel}} \zeta_{\text{red}} \zeta_{\text{ctrl}}, \quad \zeta_{\bullet} \geq 1.$$

ζ_{speed} :

finite-time premium (non-quasi-static operation).

ζ_{rel} :

reliability normalization; $\zeta_{\text{rel}} = (1 - H_b(p_e)/\ln 2)^{-1}$.

ζ_{red} :

redundancy / proofreading (repeated reads, majority voting).

ζ_{ctrl} :

sensing / actuation & housekeeping (standing loads).

The product form gives the log-additive budget

$$\ln \zeta = \ln \zeta_{\text{speed}} + \ln \zeta_{\text{rel}} + \ln \zeta_{\text{red}} + \ln \zeta_{\text{ctrl}}.$$

Power-priced throughput density. Reading dissipation in informational units uses the audited tariff as a conversion:

$$\Psi_b(x, t) \equiv \frac{\sigma_s(x, t) T(x, t)}{\varepsilon_b} \quad [\text{bit}/(\text{m}^3 \text{s})]. \quad (23)$$

In steady, isothermal domains,

$$\int_V \Psi_b dV = \frac{\int_V \sigma_s T dV}{\varepsilon_b} = \frac{P_{\text{diss}}}{\varepsilon_b} = \frac{P_{\text{flow}}}{\varepsilon_b}. \quad (24)$$

Thus Ψ_b provides a unit-consistent exchange rate between dissipation and reliably decodable structure: every watt of hydraulic power “purchases” $1/\varepsilon_b$ reliable bits per second at the audited reliability. With $\varepsilon_b = \zeta k_B T \ln 2$ the audit temperature cancels in $\Psi_b = \sigma_s/(\zeta k_B \ln 2)$, so—at fixed audit—only the dissipation density σ_s and the overhead factor ζ govern the interior budget; larger ζ tightens the budget linearly. The integral identity (24) then converts any measurement of hydraulic power into a domain-level bit budget by a single division by ε_b . In heterogeneous settings with a spatially varying tariff, the same logic yields $\int_V \sigma_s T/\varepsilon_b(x) dV$: dissipation weighted by the local price field, which is precisely the interior quantity optimized in the domain program.

METHODS: PROOF OF THE GROWTH-CONE BOUND

This section states explicit premises and derives the instantaneous two-face bound on the rate of creating stably maintained, reliably decodable distinctions inside a space-time control volume.

Assumptions (A1–A4). Let V be a domain with (time-dependent) boundary Σ_t , and let $I(t) = \int_V \iota(x, t) dV$ count ϵ -reliable, stably stored distinctions at the audit’s resolution.

(A1) *Audit & tariff.* $\varepsilon_b(x, t) = \zeta(x, t) k_B T(x, t) \ln 2$ with $\zeta \geq 1$ measured as in (21)–(22).

(A2) *Information share of dissipation.* There exists a measurable density $\dot{I}_v(x, t)$ [$\text{bit s}^{-1} \text{m}^{-3}$] of reliably executed operations such that the information-processing share of entropy production covers the tariff,

$$\sigma_s^{(\text{info})}(x, t) \geq \frac{\varepsilon_b(x, t)}{T(x, t)} \dot{I}_v(x, t). \quad (25)$$

(A3) *Reliable boundary communication.* Across Σ_t , physical channels operated at blocklength n and error ϵ deliver reliable rate density $C_\epsilon(n; x, t)$ [$\text{bit s}^{-1} \text{m}^{-2}$].

(A4) *Stock of distinctions.* $I(t)$ evolves by interior creation and boundary inflow; $\dot{I}(t) \leq \int_V \dot{I}_v dV +$ (reliably decodable inflow across Σ_t).

Lemma 1 (interior cut). Integrating (25) over V and using $\int_V \sigma_s^{(\text{info})} \leq \int_V \sigma_s$ yields

$$\int_V \dot{I}_v dV \leq \int_V \frac{\sigma_s T}{\varepsilon_b} dV = \int_V \Psi_b dV.$$

Since the rate of growth of the stock cannot exceed the rate of reliable operations,

$$\dot{I}(t) \leq \int_V \Psi_b(x, t) dV. \quad (26)$$

Lemma 2 (boundary cut). Let $M(t, \Delta t)$ be the reliably decodable message entering through Σ_t during $[t, t + \Delta t]$. By data processing and the reliability specification,

$$\mathbb{E}[\Delta I] \leq \Delta t \int_{\Sigma_t} C_\epsilon(n; x, t) dA.$$

Dividing by Δt and sending $\Delta t \downarrow 0$ gives

$$\dot{I}(t) \leq \int_{\Sigma_t} C_\epsilon(n; x, t) dA. \quad (27)$$

Theorem (Growth-cone). Combining (26) and (27) yields the instantaneous bound

$$\frac{d}{dt} \int_V \iota dV \leq \min \left\{ \int_V \Psi_b(x, t) dV, \int_{\Sigma_t} C_\epsilon(n; x, t) dA \right\}.$$

In a steady, isothermal node, $\int_V \Psi_b dV = P_{\text{diss}}/\varepsilon_b = P_{\text{flow}}/\varepsilon_b$.

Finite-blocklength approximation (for C_ϵ). With channel density $\rho_{\text{ch}}(x, t)$, symbol rate W , asymptotic capacity C (bit/s/use), and dispersion V , the normal approximation gives

$$C_\epsilon(n; x, t) = \rho_{\text{ch}}(x, t) W(x, t) \left[C - \sqrt{V/n} Q^{-1}(\epsilon) \right]_+,$$

with Q^{-1} the Gaussian quantile and $[a]_+ \equiv \max\{a, 0\}$. Equality in the growth-cone requires: (i) the nonlimiting face is slack (e.g., boundary not rate-limiting when the interior face is active), (ii) the limiting face operates reversibly at the audit’s reliability, and (iii) no additional finite-time or idle-duty overheads beyond the audited ζ erode the budget.

APPENDIX: RHEOLOGY DETAILS AND GENERAL n

This appendix states, in a compact and logically ordered form, the exact consequences of (i) a radius-dependent viscosity $\mu = \mu(r)$ and (ii) a generalized hydraulic exponent n in the per-length dissipation $P_{\text{flow}} \propto Q^2 r^{-n}$. All results are derived at a single node with fixed daughter demands (Q_1, Q_2) and $Q_0 = Q_1 + Q_2$.

Exact stationarity with $\mu(r)$. At fixed Q_i , the node objective is

$$\mathcal{L}(\mathbf{r}) = \sum_{i=0}^2 \frac{8l_i}{\pi} \mu(r_i) \frac{Q_i^2}{r_i^4} + \Lambda \sum_{i=0}^2 c_i l_i r_i^m.$$

Taking $\partial \mathcal{L} / \partial r_i = 0$ at fixed Q_i gives

$$\frac{8l_i}{\pi} Q_i^2 [\mu'(r_i) r_i^{-4} - 4\mu(r_i) r_i^{-5}] + \Lambda c_i l_i m r_i^{m-1} = 0.$$

After cancelling $l_i > 0$ and rearranging, the exact branchwise invariant reads

$$\frac{Q_i^2}{c_i r_i^{m+4}} = \frac{\pi m \Lambda}{8 [4\mu(r_i) - r_i \mu'(r_i)]} \equiv \kappa_{\text{eff}}(r_i), \quad (28)$$

which reduces to the constant- μ result when $\mu'(r) \equiv 0$. The combination $D(r) \equiv 4\mu(r) - r\mu'(r)$ is the only rheological factor that enters the invariant.

Local flow–radius slope. From (28), $Q^2 \propto c r^{m+4} / D(r)$. A logarithmic derivative with respect to $\ln r$ yields the exact local slope

$$\alpha_{\text{eff}}(r) \equiv \frac{d \ln Q}{d \ln r} = \frac{1}{2} \left[(m+4) - \frac{d}{d \ln r} \ln D(r) \right]. \quad (29)$$

Hence any increase of $\mu(r)$ with r (making $D'(r) > 0$) depresses α_{eff} below $(m+4)/2$, and any decrease elevates it above that value.

Slow-variation approximation. Write $D(r) = 4\mu(r) [1 - \xi(r)]$ with $\xi(r) \equiv r\mu'(r)/(4\mu(r))$. If $|\xi| \ll 1$ and $d\xi/d \ln r$ is small,

$$\frac{d}{d \ln r} \ln D(r) = \frac{d \ln \mu}{d \ln r} + \mathcal{O}\left(\xi, \frac{d\xi}{d \ln r}\right),$$

and (29) reduces to

$$\alpha_{\text{eff}}(r) = \frac{m+4}{2} - \frac{1}{2} \frac{d \ln \mu}{d \ln r} + \mathcal{O}\left(\xi, \xi^2, \frac{d\xi}{d \ln r}\right). \quad (30)$$

The sign and magnitude of the logarithmic slope of $\mu(r)$ therefore give an immediate, quantitative shift relative to the Poiseuille value $(m+4)/2$.

Priced–shear invariant. For laminar flow the wall shear is $\tau_w = 4\mu(r) Q / (\pi r^3)$. Eliminating Q in favor of (28) yields the branch-independent scalar

$$\mathcal{S}_i \equiv \frac{\tau_{w,i}}{\sqrt{c_i}} \frac{\sqrt{4\mu(r_i) - r_i \mu'(r_i)}}{\mu(r_i)} r_i^{\frac{2-m}{2}} = \sqrt{\frac{2m\Lambda}{\pi}}, \quad (31)$$

which is identical for $i = 0, 1, 2$. Two corollaries (equal c_i). If $\mu' \equiv 0$: for $m=2$ the wall shear is constant across branches; for $m=1$ the product $\tau_w r^{1/2}$ is constant.

General hydraulic exponent n . Let the per-length dissipation scale as $Q^2 r^{-n}$ (Poiseuille $n=4$; slip/non-Newtonian $n \neq 4$). The KKT condition at fixed Q gives, in place of the Poiseuille derivative,

$$\frac{\partial}{\partial r} (Q^2 r^{-n}) + \Lambda c m r^{m-1} = 0,$$

so the branchwise invariant becomes $Q^2 r^{-n} \propto r \partial_r (c r^m) = c m r^m$, and

$$Q \propto \sqrt{c} r^{\frac{m+n}{2}} \implies \alpha = \frac{m+n}{2}.$$

Angles remain governed solely by the translation stationarity $\sum_i c_i r_i^m \mathbf{e}_i = \mathbf{0}$ (independent of n), while a uniform dilation $r \mapsto (1+\epsilon)r$ at the interior optimum yields the homogeneity (equipartition) relation

$$n P_{\text{flow}} = m P_{\text{struct}}, \quad P_{\text{struct}} \equiv \Lambda \mathcal{B}, \quad (32)$$

so the optimal fraction of total power in dissipation is $m/(m+n)$ and the fraction in structure is $n/(m+n)$.

In summary, the rheological dependence enters the node problem through the single factor $D(r) = 4\mu - r\mu'$ in the exact invariant (28); this controls both the local slope $\alpha_{\text{eff}}(r)$ via (29)–(30) and the priced-shear invariant (31), while the geometrical laws for angles and the homogeneity-based equipartition (32) remain unchanged by rheology.

APPENDIX: GEOMETRY-ONLY TARIFF TOMOGRAPHY

This appendix shows how to infer the *relative* tariffs c_1/c_0 and c_2/c_0 from a single node when only $(r_0, r_1, r_2, \theta_{12})$ are measured and no control-layer audit is available. Throughout $m > 0$ is fixed, $\alpha = \frac{m+4}{2}$, radii are strictly positive, and $0 < \theta_{12} < \pi$.

Setup and normalization. Let

$$k_1 \equiv \frac{c_1}{c_0}, \quad k_2 \equiv \frac{c_2}{c_0}, \quad x \equiv \sqrt{k_1} > 0, \quad y \equiv \sqrt{k_2} > 0.$$

Define the compact notation

$$A = r_1^\alpha, \quad B = r_2^\alpha, \quad C = r_0^\alpha, \quad W_1 = r_1^m, \quad W_2 = r_2^m.$$

The two node laws are

$$\text{(weighted Murray)} \quad C = xA + yB, \quad (33)$$

$$\text{(cosine law)} \quad \cos \theta_{12} = \frac{r_0^{2m} - x^4 W_1^2 - y^4 W_2^2}{2x^2 y^2 W_1 W_2} \quad (34)$$

Equation (33) expresses y as an affine function of x :

$$y(x) = \frac{C - xA}{B}, \quad 0 < x < \frac{C}{A}, \quad (35)$$

where the open interval ensures $x > 0$ and $y(x) > 0$.

Single-variable reduction. Substituting (35) into (34) yields a scalar equation for x :

$$\Phi(x) \equiv \frac{r_0^{2m} - x^4 W_1^2 - y(x)^4 W_2^2}{2x^2 y(x)^2 W_1 W_2} - \cos \theta_{12} = 0, \quad (36)$$

with $x \in \left(0, \frac{C}{A}\right)$.

Clearing denominators shows that Φ is a real quartic rational function of x ; it is smooth on the admissible interval.

Existence, admissible bracket, and uniqueness. The mapping $x \mapsto y(x)$ is strictly decreasing on $(0, \frac{C}{A})$ and keeps (x, y) in $\mathbb{R}_{>0}^2$. At the left endpoint, $x \downarrow 0$ and $y \uparrow C/B$; at the right endpoint, $x \uparrow C/A$ and $y \downarrow 0$. In both limits the denominator $2x^2 y^2 W_1 W_2$ of (36) vanishes while the numerator remains finite and changes sign, so Φ crosses the prescribed constant $\cos \theta_{12} \in (-1, 1)$. Hence there exists at least one root $x^* \in (0, C/A)$. On this interval the function $x \mapsto \Phi(x)$ is strictly monotone (the derivative has a fixed sign; a short calculation uses that $y'(x) = -A/B < 0$ and that the two terms $\propto x^2$ and $\propto y(x)^2$ in the denominator enforce one sign change), so the root is unique. A robust solver is therefore any bracketed one-dimensional method (e.g., bisection or Brent) on $(0, C/A)$.

Reconstruction. Given x^* , set

$$y^* = y(x^*) = \frac{C - x^* A}{B}, \quad \frac{c_1}{c_0} = (x^*)^2, \quad \frac{c_2}{c_0} = (y^*)^2.$$

Because only the *ratios* are identified, the absolute scale of (c_0, c_1, c_2) remains undetermined, as expected.

Closed form in the near-symmetric case. If $r_1 = r_2 \equiv r$ (hence $A = B = r^\alpha$, $W_1 = W_2 = r^m$), set

$$S \equiv \frac{C}{A} = \left(\frac{r_0}{r}\right)^\alpha, \quad R \equiv \left(\frac{r_0}{r}\right)^{2m}.$$

Then $x + y = S$ from (33). Let $p \equiv xy$. Using $x^4 + y^4 = (x^2 + y^2)^2 - 2x^2 y^2 = (S^2 - 2p)^2 - 2p^2$, equation (34) reduces to a quadratic for p :

$$(1 + \cos \theta_{12}) p^2 - 2S^2 p + \frac{1}{2}(S^4 - R) = 0.$$

Choose the physically admissible root $p \in (0, S^2/4)$ (ensures $x, y > 0$), then recover

$$x, y = \frac{S \pm \sqrt{S^2 - 4p}}{2}, \quad \frac{c_1}{c_0} = x^2, \quad \frac{c_2}{c_0} = y^2.$$

This symmetric closed form is numerically stable and avoids any iterative solve.

Practical notes (conditioning and scaling). To improve numerical conditioning, it is beneficial to rescale by r_2 : set $\tilde{r}_i = r_i/r_2$ so that $B = 1$ and $W_2 = 1$. The admissible bracket then simplifies to $x \in (0, C/A)$ with $y = C - xA$. Evaluating Φ

via (36) in this normalized frame keeps all intermediate quantities $O(1)$ even when r_i span several decades. Measurement errors in $(r_0, r_1, r_2, \theta_{12})$ propagate to $(c_1/c_0, c_2/c_0)$ through (A, B, C, W_1, W_2) and the scalar map $x \mapsto \Phi(x)$; first-order sensitivities follow by differentiating (36) implicitly and using (35).

APPENDIX: TUR REMARK

For an appropriate stationary current J , the thermodynamic uncertainty relation (TUR) states

$$\frac{\text{Var}[J]}{\langle J \rangle^2} \geq \frac{2}{\Sigma_{\text{tot}}/k_B}.$$

Since $\Sigma_{\text{tot}} \geq \Sigma_{\text{info}} \geq \zeta k_B \ln 2 \int \dot{I} dt$, it follows that $2/(\zeta \ln 2 \int \dot{I} dt)$ is merely an *upper bound on this lower bound*. Consequently, no *guaranteed* TUR-type constraint can be written solely in terms of $\int \dot{I} dt$ and ζ without further dynamical assumptions; TUR is therefore not used here to produce quantitative bounds expressed only in $\int \dot{I} dt$.

DATA USE AND LICENSING (HRF)

This study uses the High-Resolution Fundus (HRF) Image Database provided by the Pattern Recognition Lab, Friedrich-Alexander-Universität Erlangen-Nürnberg (FAU). The HRF database is released under the Creative Commons Attribution 4.0 International (CC BY 4.0) license, which permits sharing and adaptation with appropriate credit and a link to the license. Dataset page: [HRF \(FAU Pattern Recognition Lab\)](#); license: [CC BY 4.0](#). Accessed 10 Nov 2025.

Availability. All analysis code, configuration files, and figure-generation scripts used in this work are available in the public *EPICproject* repository: github.com/JustinBen0131/EPICproject (tag v2-arxiv). The repository contains the exact pipeline used to produce Figs. 1–3, together with text preregistration fragments and run-time parameters. Raw fundus images are not redistributed; they must be obtained from HRF under the CC BY 4.0 license. A minimal node-level CSV bundle (radii, angles, per-node m and $R(m)$, and QC flags) is provided as ancillary material to this arXiv submission.

ACKNOWLEDGMENTS

The High-Resolution Fundus (HRF) images were created at the Pattern Recognition Lab, Friedrich-Alexander-Universität Erlangen-Nürnberg, with cooperating clinical partners acknowledged on the HRF project page. The author acknowledges these institutions for making the HRF data publicly available.

[1] S. R. de Groot and P. Mazur, *Non-Equilibrium Thermodynamics* (Dover (reprint) / North-Holland, 1962).

[2] L. Onsager, *Physical Review* **37**, 405 (1931).

- [3] L. Onsager, *Physical Review* **38**, 2265 (1931).
- [4] U. Seifert, *Reports on Progress in Physics* **75**, 126001 (2012).
- [5] C. D. Murray, *Proceedings of the National Academy of Sciences* **12**, 207 (1926).
- [6] C. D. Murray, *The Journal of General Physiology* **9**, 835 (1926).
- [7] T. F. Sherman, *The Journal of General Physiology* **78**, 431 (1981).
- [8] M. Zamir, *Journal of Theoretical Biology* **62**, 227 (1976).
- [9] A. Bérut, A. Arakelyan, A. Petrosyan, S. Ciliberto, R. Dillenschneider, and E. Lutz, *Nature* **483**, 187 (2012).
- [10] F. M. White, *Viscous Fluid Flow*, 3rd ed. (McGraw–Hill, 2006).
- [11] H. Bruus, *Theoretical Microfluidics*, Oxford Master Series in Physics (Oxford University Press, 2008).
- [12] D. R. Emerson, K. Cieřlicki, X. Gu, and R. W. Barber, *Lab on a Chip* **6**, 447 (2006).
- [13] A. K. da Silva, S. Lorente, and A. Bejan, *Journal of Applied Physics* **96**, 1709 (2004).
- [14] A. R. Pries, D. Neuhaus, and P. Gaetgens, *American Journal of Physiology-Heart and Circulatory Physiology* **263**, H1770 (1992).
- [15] T. W. Secomb, *Comptes Rendus Physique* **14**, 470 (2013).
- [16] M. Ascolese, A. Grillo, M. Carfagna, G. Rusciano, and A. Sasso, *Biophysical Reviews* **11**, 827 (2019).
- [17] D. Weaire and S. Hutzler, *The Physics of Foams* (Oxford University Press, 1999).
- [18] R. B. Bird, W. E. Stewart, and E. N. Lightfoot, *Transport Phenomena*, 2nd ed. (John Wiley & Sons, 2007).
- [19] R. P. Chhabra and J. F. Richardson, *Non-Newtonian Flow and Applied Rheology*, 2nd ed. (Butterworth–Heinemann, 2008).
- [20] R. Landauer, *IBM Journal of Research and Development* **5**, 183 (1961).
- [21] T. M. Cover and J. A. Thomas, *Elements of Information Theory*, 2nd ed. (Wiley, 2006).
- [22] Y. Polyanskiy, H. V. Poor, and S. Verdú, *IEEE Trans. Inf. Theory* **56**, 2307 (2010).
- [23] Pattern Recognition Lab, Friedrich-Alexander-Universität Erlangen-Nürnberg, *High-resolution fundus (hrf) image database* (2013), accessed 10 Nov 2025.
- [24] A. Budai, R. Bock, A. Maier, J. Hornegger, and G. Michelson, *International Journal of Biomedical Imaging* **2013**, 154860 (2013).
- [25] J. Odstrěilík, R. Kolář, P. Janša, *et al.*, *IET Image Processing* **7**, 373 (2013).
- [26] Y. Sato, S. Nakajima, N. Shiraga, H. Atsumi, S. Yoshida, T. Koller, G. Gerig, and R. Kikinis, *Medical Image Analysis* **2**, 143 (1998).
- [27] N. Otsu, *IEEE Transactions on Systems, Man, and Cybernetics* **9**, 62 (1979).
- [28] T. Y. Zhang and C. Y. Suen, *Communications of the ACM* **27**, 236 (1984).
- [29] P. F. Felzenszwalb and D. P. Huttenlocher, *Theory of Computing* **8**, 415 (2012).
- [30] J. Bennett, EPICproject: Code and analysis for “murray’s law as an entropy-per-information-cost extremum”, <https://github.com/JustinBen0131/EPICproject> (2025), git tag v2-arxiv.
- [31] B. Efron and R. J. Tibshirani, *An Introduction to the Bootstrap* (Chapman and Hall/CRC, 1993).
- [32] N. Cliff, *Psychological Bulletin* **114**, 494 (1993).
- [33] C. D. Murray, *Proceedings of the National Academy of Sciences of the USA* **12**, 207 (1926).
- [34] J. D. Gibbons and S. Chakraborti, *Nonparametric Statistical Inference*, 5th ed. (Chapman and Hall/CRC, 2011).
- [35] J. Staal, M. D. Abràmoff, M. Niemeijer, M. A. Viergever, and B. van Ginneken, *IEEE Transactions on Medical Imaging* **23**, 501 (2004).
- [36] A. Hoover, V. Kouznetsova, and M. Goldbaum, *IEEE Transactions on Medical Imaging* **19**, 203 (2000).
- [37] Kingston University London, Retinal Imaging Group, Chase_db1 retinal image database, <https://blogs.kingston.ac.uk/retinal/chasedb1/> (2011), accessed for dataset identification.
- [38] H. Theil, *Nederl. Akad. Wetensch., Proc.* **53**, 386 (1950).
- [39] P. K. Sen, *Journal of the American Statistical Association* **63**, 1379 (1968).
- [40] S. Boyd and L. Vandenberghe, *Convex Optimization* (Cambridge University Press, 2004) first-order optimality and homogeneity; see Chs. 2–4.
- [41] T. M. Apostol, *Calculus, Vol. II: Multi-Variable Calculus and Linear Algebra with Applications to Differential Equations and Probability* (Wiley, 1967) euler’s theorem for homogeneous functions; see Sec. 14.
- [42] A. Bejan, *Philosophical Transactions of the Royal Society B* **365**, 1335 (2010).
- [43] M. Born and E. Wolf, *Principles of Optics: Electromagnetic Theory of Propagation, Interference and Diffraction of Light*, 7th ed. (Cambridge University Press, 1999).
- [44] L. D. Landau and E. M. Lifshitz, *Electrodynamics of Continuous Media*, 2nd ed., Course of Theoretical Physics, Vol. 8 (Butterworth–Heinemann, 1984).